Applied Catalysis B: Environmental 305 (2022) 121031

Contents lists available at ScienceDirect

Applied Catalysis B: Environmental

journal homepage: www.elsevier.com/locate/apcatb

Efficient visible light initiated one-pot syntheses of secondary amines from nitro aromatics and benzyl alcohols over Pd@NH_2-UiO-66(Zr)

Mingming Hao, Zhaohui Li *

Research Institute of Photocatalysis, State Key Laboratory of Photocatalysis on Energy and Environment, College of Chemistry, Fuzhou University, Fuzhou 350116, PR China

ARTICLE INFO

Keywords:
Nitro compounds
Alcohols
Secondary amines
Pd@NH_2-UiO-66(Zr)
Visible light

ABSTRACT

Pd@NH_2-UiO-66(Zr), with small-sized Pd nanoparticles encapsulated inside the cavities of NH_2-UiO-66(Zr), was obtained via a double-solvent impregnation followed by a photoreduction process, which shows superior activity for the visible light initiated syntheses of secondary amines from nitro compounds and alcohols, via a sequential photocatalytic hydrogenation of nitro compounds/dehydrogenation of alcohols, condensation of amines and aldehydes to imines, and the hydrogenation of imines. Simultaneous consumption of photogenerated electrons/holes in the photocatalytic hydrogenation of nitro compounds to amines and dehydrogenation of alcohols to aldehydes promotes the whole reaction. Due to the confinement effect of the cavity and the small-sized Pd nanoparticles, Pd@NH_2-UiO-66(Zr) shows significantly superior performance as compared with Pd/NH_2-UiO-66(Zr), in which larger Pd nanoparticles are deposited on the surface. This study provides an efficient and green strategy for the production of secondary amines and highlights the great potential of using M/MOFs nanocomposites as multifunctional catalysts for light induced one-pot tandem reactions.

1. Introduction

One-pot tandem/cascade reactions, which enable multistep reactions to be realized in one pot, represent a promising direction for future chemical synthesis because they can avoid the separation of intermediates, save processing time and reduce the production of wastes [1–3]. In particular, light-induced tandem/cascade reactions have attracted a great deal of attentions since the introduction of light irradiations into the reaction systems can enable these tandem/cascade reactions to be carried out in mild condition and thus conform to the concepts of green chemistry [4,5]. Multifunctional photocatalysts required by these light-induced tandem/cascade reactions not only should possess superior photocatalytic activity, but also should contain different isolated catalytic active sites to work independently and synergistically. Metal-Organic Frameworks (MOFs), a class of crystalline micro-/mesoporous hybrid materials with extended 3D networks, are emerging as promising multifunctional photocatalysts due to their tunable light absorption and the existence of a variety of catalytic active sites in their structures [6–14]. In addition, due to the presence of surface anchoring sites and tunable pores/cages in their structures, MOFs can also be a good platform for assembling different catalytic active components, either by anchoring them on the surface or encapsulating inside the pores, for developing multifunctional MOF-based photocatalysts [15–24]. Among all these multifunctional MOF-based catalysts, MNPs/MOFs (MNPs = metal nanoparticles) nanocomposites have been the most extensively studied since both MOFs and MNPs play important roles in heterogeneous catalysis [15,19,20]. In particular, the cavities of MOFs can be used as excellent nanoreactors for size controllable growth of MNPs. As a result, by coupling (photo)catalysis of MOFs with that of MNPs, MNPs/MOFs nanocomposites have shown promising application in a variety of light induced tandem/cascade reactions [4,25].

Direct N-alkylation of primary amines with alcohols as the alkylating agents to obtain secondary amines is an important reaction since N-alkyl amines and their derivatives are versatile synthons for the synthesis of agrochemicals, pharmaceuticals and bioactive molecules [26]. Previous studies have found that this reaction can be realized under mild visible light irradiations over several Pd/photocatalysts nanocomposites, via a sequential dehydrogenation of alcohols to aldehydes, condensation of amines and aldehydes to imines, and the hydrogenation of imines (Scheme 1(i, ii, iii)) [27–32]. The light-induced N-alkylation of amines with alcohols is green since it can be carried out under mild visible light

* Corresponding author.
E-mail address: zhaohuili@fzu.edu.cn (Z. Li).

https://doi.org/10.1016/j.apcatb.2021.121031
Received 21 November 2021; Accepted 20 December 2021
Available online 22 December 2021

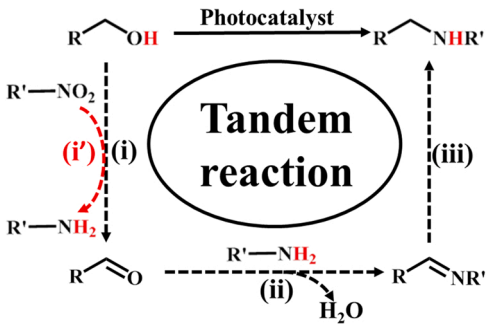

Scheme 1. Light-induced one-pot tandem reaction to produce secondary amines.

irradiation, with water produced as the only byproduct. However, the limitation lies in that the substrate amines are not stable and are easily oxidized, which complicate the reactions [33]. Considering that nitro compounds are more stable, it would be ideal to directly use nitro compounds instead of amines as the starting material to prepare secondary amines. This reaction protocol is feasible since the nitro compounds can be hydrogenated to amines in the presence of suitable hydrogen donors like alcohols, while the dehydrogenation of alcohols is involved in the N-alkylation reactions (Scheme 1(i')) [34–37]. In particular, the coupling of the photocatalytic hydrogenation of nitro compounds to amines and the photocatalytic dehydrogenation of alcohols consumes the photogenerated electrons and holes in the meantime, which is expected to promote the whole tandem reaction since previous studies revealed that the photocatalytic dehydrogenation of alcohols is the rate limiting step of the whole N-alkylation of amines reactions [28].

Herein, we reported the application of Pd@NH_2-UiO-66(Zr) nanocomposite, with small-sized Pd nanoparticles encapsulated inside the cavities of NH_2-UiO-66(Zr), for one-pot syntheses of secondary amines by reacting nitro compounds with alcohols under visible light. NH_2-UiO-66(Zr) is an amine-functionalized Zr-based MOF obtained by substituting 1,4-dicarboxybenzene (BDC) in UiO-66(Zr)($(Zr_6O_4(OH)_4(CO_2)_{12}$) with 2-amino-benzene-1,4-dicarboxylate (NH_2-BDC), which has already been applied in a variety of photocatalytic reactions under visible light [38,39]. Pd@NH_2-UiO-66(Zr) was obtained via a double-solvent impregnation of $Pd(NO_3)_2$ in NH_2-UiO-66(Zr), followed by a photoreduction process to obtain small-sized Pd nanoparticles encapsulated inside the cavities of NH_2-UiO-66(Zr). The as-obtained Pd@NH_2-UiO-66(Zr) shows superior activity for the one-pot syntheses of secondary amines from the reaction between nitro compounds and alcohols under visible light. As compared with Pd/NH_2-UiO-66(Zr) in which larger Pd nanoparticles were deposited on the surface of NH_2-UiO-66(Zr), Pd@NH_2-UiO-66(Zr) shows significantly superior performance and higher stability during the reaction. This study not only provides an efficient, green and cost effective strategy for the production of secondary amines, but also offers some guidance for the rational design of multifunctional MOF-based photocatalysts for efficient one-pot cascade/tandem reaction.

2. Experimental

2.1. Preparations

All the reagents were commercially available and used without further purification. NH_2-UiO-66(Zr) was prepared from zirconium tetrachloride ($ZrCl_4$) and 2-aminoterephthalate (H_2ATA) following a previous reported procedure [40].

Pd@NH_2-UiO-66(Zr) was prepared by a double-solvent impregnation approach followed by a photoreduction process [41]. In order to introduce the precursor of Pd into the cavities of NH_2-UiO-66(Zr), 100 mg of activated NH_2-UiO-66(Zr) was suspended in 20 mL dry n-hexane and sonicated for about 1 h until it became a homogeneous suspension. Subsequently, 25 μL of $Pd(NO_3)_2$•2 H_2O (0.75 M) aqueous solution was added dropwisely using a pipette under vigorous stirring. After continuously stirred for 2 h, the solid was isolated from the supernatant by decanting, washed with ethanol, and dried under vacuum. The as-obtained solid product was then suspended in degassed anhydrous methanol (10 mL) and was irradiated under visible light for 4 h. The resultant sample was filtered, washed with methanol for several times and dried under vacuum overnight.

For comparison, Pd/NH_2-UiO-66(Zr) was synthesized employing a conventional single solvent impregnation approach combined with a photoreduction process. 25 μL $Pd(NO_3)_2$•2 H_2O (0.75 M) aqueous solution was added to the degassed anhydrous methanol (10 mL) suspension containing 100 mg of NH_2-UiO-66(Zr) under N_2. The as-obtained suspension was then irradiated under visible light for 4 h. The resultant solid was filtered, washed with methanol, and dried overnight at 60 °C in an oven.

2.2. Characterizations

Power X-ray diffraction (XRD) patterns were characterized on a Rigaku SmartLab rotation anode X-ray diffractometer with graphite-monochromated Cu Kα radiation. XRD patterns were scanned over the angular range of 3–60° (2θ) with a step size of 0.02°. The transmission electron microscopy (TEM) and high-resolution transmission electron microscopy (HRTEM) images were measured on a JEOL model JEM 2010 EX instrument. X-ray photoelectron spectroscopy (XPS) measurements were performed on a PHI Quantum 2000 XPS system (PHI, USA) with a monochromatic Al Kα source and a charge neutralizer. All the binding energies were referenced to the C1s peak at 284.6 eV of the surface adventitious carbon. The amount of Pd was determined on an inductively coupled plasma emission spectrometer (ICP, PerkinElmer Optima 8000). UV–visible diffuse reflectance spectra (UV-DRS) of the powders were obtained with $BaSO_4$ used as a reflectance standard. BET surface area was determined on an ASAP 2020 M apparatus (Micromeritics Instrument Corp., USA). The samples were degassed under vacuum at 200 °C for 10 h and then measured at − 196 °C.

2.3. Catalytic reactions

The photocatalytic reactions were carried out in a sealed reaction tube with a 300 W Xe arc lamp (Beijing Perfect light, Microsolar 300) in room temperature. Typically, the catalyst (10 mg) and nitro compounds (0.1 mmol) were suspended in a mixture of alcohol and acetonitrile (CH_3CN) (2 mL). The suspension was degassed and saturated with N_2 to remove the dissolved O_2 before the reaction. Then the reaction tube was irradiated with a 300 W Xe arc lamp equipped with an IR-cut filter to remove all irradiation with wavelengths greater than 800 nm. After the reaction, the resultant suspension was filtered through a porous membrane (20 μm in diameter) and the filtrate was analyzed by GC-MS and GC-FID (Shimadzu GC-2014) equipped with an HP-5 capillary column. The GC spectra of the standard samples were shown in Fig. S1(a).

3. Result and discussion

3.1. Syntheses and characterizations of Pd@NH_2-UiO-66(Zr)

NH_2-UiO-66(Zr) was obtained solvothermally from $ZrCl_4$ and H_2ATA in DMF according to the literature [40]. The as-obtained NH_2-UiO-66(Zr) shows similar XRD patterns and comparable BET surface area (964 m^2/g) to those reported previously, indicating NH_2-UiO-66(Zr) obtained has high quality (Fig. 1(a) and Fig. S2(a)). To obtain Pd@NH_2-UiO-66(Zr), a double-solvent impregnation approach was applied to introduce the Pd precursor into the cavities of NH_2-UiO-66(Zr), which followed by a photoreduction process to obtain small-sized Pd nanoparticles encapsulated inside the cavities of NH_2-UiO-66(Zr).

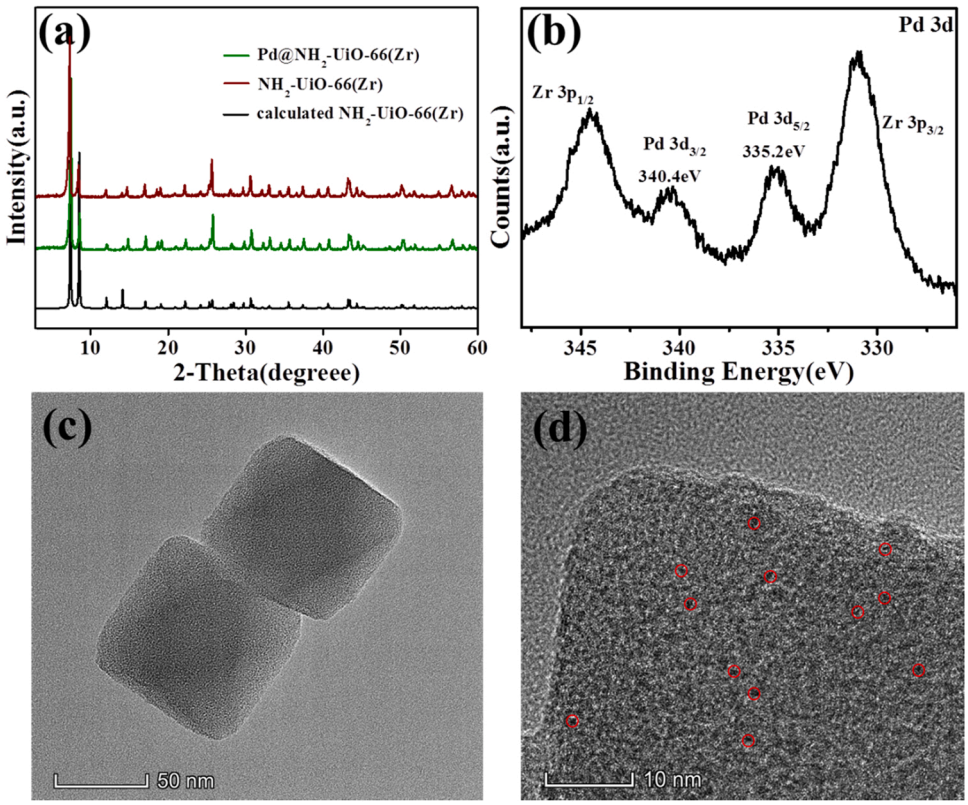

Fig. 1. (a) XRD patterns of Pd@NH_2-UiO-66(Zr), NH_2-UiO-66(Zr) and calculated NH_2-UiO-66(Zr); (b) XPS spectrum of Pd@NH_2-UiO-66(Zr) in Pd 3d region; (c) TEM and (d) HRTEM images of Pd@NH_2-UiO-66(Zr).

The as-obtained Pd@NH_2-UiO-66(Zr) shows similar XRD patterns to bare NH_2-UiO-66(Zr), indicating that the structure of NH_2-UiO-66(Zr) is well maintained after the metal encapsulation process (Fig. 1(a)). Although no diffraction peaks corresponding to metallic Pd are observed, probably due to it low loading amount or homogeneous dispersion, the existence of Pd^0 is confirmed by the XPS analyses (Fig. 1 (b)). The XPS spectrum in Pd 3d region shows two peaks at 335.2 and 340.4 eV, corresponding to Pd $3d_{5/2}$ and Pd $3d_{3/2}$ of Pd^0 respectively, which illustrates that Pd^{2+} was reduced to Pd NPs via the photoreduction process over NH_2-UiO-66(Zr). TEM image shows that the morphology of Pd@NH_2-UiO-66(Zr) nanocomposites are octahedrons, with smooth surface and a dimension of about 100 nm, suggesting that no Pd NPs are deposited on the external surface of NH_2-UiO-66(Zr) (Fig. 1(c)). HRTEM image further proves that Pd nanoparticles have been confined in the cavities of NH_2-UiO-66(Zr) by showing metal nanoparticles with an average diameter of around 1.0 nm regularly dispersed in Pd@NH_2-UiO-66(Zr) (Fig. 1(d)). The use of double-solvent impregnation approach to introduce metal precursors into the cavities of the MOFs and followed by different reduction processes to prepare metal NPs encapsulated inside the cavities of MOFs have already been well demonstrated [41]. In this case, for encapsulating Pd nanoparticles into the cavities of NH_2-UiO-66(Zr), aqueous $Pd(NO_3)_2$ solution was introduced into the pores of activated NH_2-UiO-66(Zr) by capillary force due to the hydrophilic nature of the inner pore environment. The later light irradiations resulted in the reduction of cavity encapsulated Pd^{2+}, in which the cavity acts like nanoreactor for controllable growth of small-sized Pd nanoparticles. The amount of Pd in Pd@NH_2-UiO-66(Zr) was determined to be ca. 1.97 wt% by ICP-OES, which is consistent with the amount of Pd introduced. The encapsulation of Pd NPs inside the cavities of NH_2-UiO-66(Zr) leads to a slight decrease of the specific surface area from the original 964 m^2/g for NH_2-UiO-66(Zr) to 832 m^2/g for Pd@NH_2-UiO-66(Zr) (Fig. S2(b)). The UV–vis DRS spectrum of the Pd@NH_2-UiO-66(Zr) shows enhanced absorption in the 200–800 nm region as compared with pristine NH_2-UiO-66(Zr) after the encapsulation of Pd nanoparticles (Fig. 2).

3.2. *Investigation on the light initiated activity for the reaction between nitrobenzene and benzyl alcohol over Pd@NH_2-UiO-66(Zr)*

To study the catalytic performance of the as-prepared Pd@NH_2-UiO-66(Zr) for synthesis of secondary amines from nitro compounds and alcohols under visible light, the reaction between nitrobenzene and benzyl alcohol was chosen as a model reaction. The reaction was initially carried out in a mixed solvent of benzyl alcohol and acetonitrile (v/v,1:1) under visible light, in which excess benzyl alcohol acts both as a reactant and a solvent. It was found that 93% of nitrobenzene was converted after irradiated for 24 h, with a yield of 81% to the desired product N-benzylaniline (Table 1, entry 1). N-benzylideneaniline (5%), aniline (4%) and benzaldehyde (2292μmol) were also produced, but no

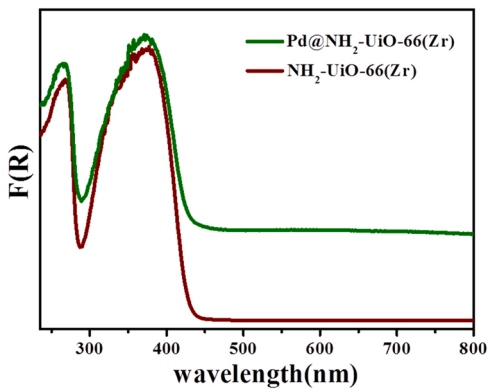

Fig. 2. UV–vis DRS spectra of NH_2-UiO-66(Zr) and Pd@NH_2-UiO-66(Zr).

Table 1
Light-induced catalytic performance for syntheses of secondary amines by nitrobenzene and benzyl alcohol under varied conditions.

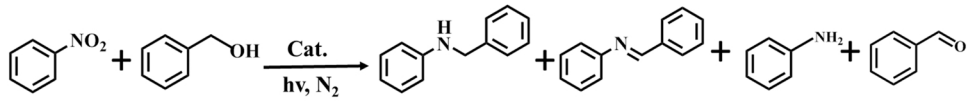

1a 2a 3a 3b 3c 3d

Entry.	Cat.	Conv. (%)	Yield. (%)			Aldehyde (μmol)
			3a	3b	3c	
1	Pd@NH_2-UiO-66(Zr)	93	81	5	4	2292
2[a]	Pd@NH_2-UiO-66(Zr)	98	95	2	1	2386
3[a,b]	Pd@NH_2-UiO-66(Zr)	89	85	1	3	483
4[c]	Pd@NH_2-UiO-66(Zr)	–	–	–	–	–
5	–	–	–	–	–	–
6	NH_2-UiO-66(Zr)	27	–	19	7	1058
7	Pd/NH_2-UiO-66(Zr)	82	59	19	4	1324
8[a,d]	Pd@NH_2-UiO-66(Zr)	94	91	1	1	12873

Reaction conditions: Cat. 10 mg, nitrobenzene 0.1 mmol, benzyl alcohol 1 mL, CH_3CN 1 mL, N_2, irradiated for 24 h. a. Irradiated for 30 h. b. benzyl alcohol 0.2 mL, CH_3CN 1.8 mL. c. Without light irradiation. d. The reaction was scaled up by 10 times.

over-alkylated tertiary amine was detected. A prolonged reaction time of 30 h led to an almost quantitative transformation of nitrobenzene (98%) with a superior yield of 95% to N-benzylaniline (Table 1, entry 2). Using lesser excess of benzyl alcohol led to a slightly lower activity. The reaction carried out using one-fifth of the original benzyl alcohol (1 mL) exhibited a slightly lower yield to N-benzylaniline (85%) after irradiated for 30 h under otherwise similar condition (Table 1, entry 3). No product was detected when the reaction was carried out in absence of either light or Pd@NH_2-UiO-66(Zr) nanocomposites (Table 1, entries 4, 5), indicating that the synthesis of secondary amines from the reaction between nitrobenzene and benzyl alcohol was induced by visible light over Pd@NH_2-UiO-66(Zr).

The time-dependent conversion of nitrobenzene and the formation of the products over Pd@NH_2-UiO-66(Zr) were shown in Fig. 3, with the GC spectra during the reaction shown in Fig. S1(b). The amount of nitrobenzene decreased, while the amount of benzaldehyde and N-benzylaniline increased steadily over irradiation time, although in different increasing profile. Both aniline and N-benzylideneaniline increased first and then decreased, with the maximum amount of aniline and N-benzylideneaniline appeared at 6 h and 12 h respectively, suggesting that both aniline and N-benzylideneaniline are the intermediates during this reaction. It is obvious that in the first 6 h, the hydrogenation of nitrobenzene to produce aniline and the dehydrogenation of benzyl alcohol to produce benzaldehyde occurred as the two main reactions since both the amount of aniline and benzaldehyde increased, together with a sharp decrease of the amount of nitrobenzene. As observed in photocatalytic hydrogenation of nitrobenzene over CQDs/$ZnIn_2S_4$, no nitrosobenzene and phenylhydroxylamine were detected, although they are considered to be intermediates in the hydrogenation of nitrobenzene to aniline according to the well-known pathways proposed by Haber [34,42]. It is either because that the hydrogenation of nitrosobenzene and phenylhydroxylamine are much faster than the reduction of nitrobenzene to produce nitrosobenzene, or nitrobenzene can be hydrogenated to produce aniline directly over Pd@NH_2-UiO-66(Zr) nanocomposites. After 6 h, the amount of aniline started to decrease, along with a rapid increase of N-benzylideneaniline and a slower rate for the production of benzaldehyde, suggesting that the condensation between aniline and benzaldehyde to form N-benzylideneaniline occurred during this period. After 12 h, the amount of N-benzylideneaniline decreased, accompanied by a rapid increase of the amount of N-benzylaniline, until 95% yield was achieved after irradiated for 30 h, illustrating the hydrogenation of N-benzylideneaniline to N-benzylaniline during this period.

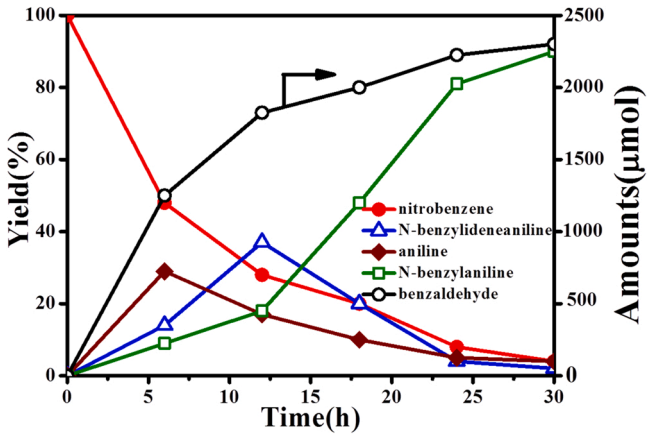

Fig. 3. Time-dependent changes of the amounts of nitrobenzene and the products during the synthesis of secondary amines by nitrobenzene and benzyl alcohol under visible light over Pd@NH_2-UiO-66(Zr).

3.3. Mechanistic studies

The time-dependent experiment clearly demonstrated that the reaction between nitrobenzene and benzyl alcohol to produce N-benzylaniline over irradiated Pd@NH_2-UiO-66(Zr) undergoes several consecutive steps. The first step is the hydrogenation of nitrobenzene to aniline, together with the dehydrogenation of benzyl alcohol to benzaldehyde, which followed by the condensation between aniline and benzaldehyde to N-benzylideneaniline and the hydrogenation of N-benzylideneaniline to N-benzylaniline. As shown in Scheme 2, this reaction is also initiated by the light irradiation over NH_2-UiO-66(Zr) to generated electrons and holes, as that proposed previously for the N-alkylation over Pd@MIL-100(Fe) [28]. The photogenerated holes can react with benzyl alcohol to generate benzaldehyde by releasing H^+, while the photogenerated electrons can transfer from NH_2-UiO-66(Zr) to the cavity encapsulated Pd NPs to form electron-rich Pd species, which subsequently reacted with the released H^+ on Pd NPs to form Pd-H active species. Subsequently, these Pd-H active species can easily react with nitrobenzene to form aniline. The condensation between the in-situ formed benzaldehyde and aniline over Lewis acidic Zr^{4+} in NH_2-UiO-66 (Zr) produce imines, which is further hydrogenated by the active Pd-H active species to generate secondary amines. Although the direct hydrogenation of nitrobenzene by the photogenerated electrons is also possible due to a more negative conduction band position of NH_2-UiO-66(Zr) (−0.73 V vs NHE) as compared with that of the reduction potential of nitrobenzene to aniline (−0.48 V vs NHE) [43],

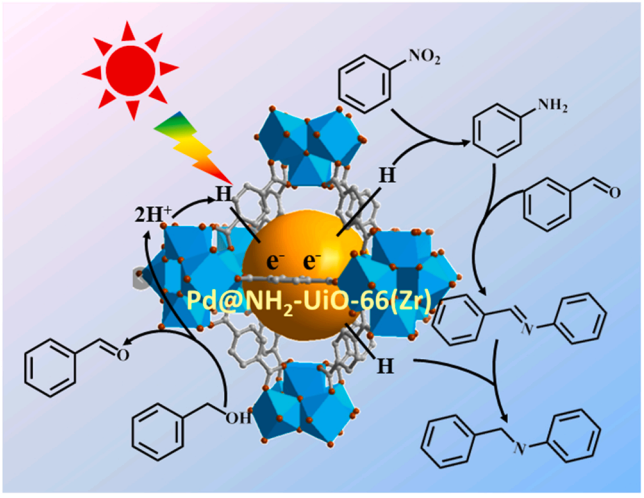

Scheme 2. Proposed mechanism for the syntheses of secondary amines by nitrobenzene and benzyl alcohol under visible light.

since the cavities encapsulated Pd nanoclusters are in close vicinity in Pd@NH_2-UiO-66(Zr), and Pd has a relatively higher work function (5.12 eV), the transfer of the photogenerated electrons from the excited MOFs to Pd nanoclusters would be more facilitated. Actually, previous study also confirmed that Pd-H is the active species for the hydrogenation of nitrobenzene to aniline under visible light over Pd/semiconductor nanocomposites [44]. Therefore, it is believed that as compared with the hydrogenation of nitrobenzene directly by the photogenerated electrons, it is more likely that Pd-H is involved in the hydrogenation of nitrobenzene in Pd@NH_2-UiO-66(Zr). It is worth noting that the amount of benzaldehyde generated in this system during the first 6 h is much higher than that observed previously when aniline was used as the substrate, with nearly 50 times of benzaldehyde detected at 6 h, suggesting that using nitrobenzene to replace aniline in the reaction greatly promoted the dehydrogenation of alcohols (Fig. S3). The simultaneous consumption of the photogenerated electrons in the hydrogenation of nitrobenzene to form aniline and the photogenerated holes for photocatalytic dehydrogenation of benzyl alcohol lead to improved generation and separation of the photogenerated charge carriers over NH_2-UiO-66(Zr) [45]. Since the photocatalytic dehydrogenation of alcohols is found to be the rate limiting step in the photocatalytic N-alkylation reaction of aniline, the use of nitrobenzene to replace the aniline can also promote the whole tandem reaction to produce secondary amines [30].

3.4. Influence of Pd nanoparticles on the performance

As shown in Table 1, only 27% of nitrobenzene was converted over bare NH_2-UiO-66(Zr) under similar condition, with the main product obtained to be N-benzylideneaniline (19%) (Table 1, entry 6), indicating that the hydrogenation of N-benzylideneaniline to N-benzylaniline occurs over Pd NPs, in consistent with our previous studies on the N-alkylation of amines over Pd@MIL-100(Fe) [28]. Since it is generally known that catalytic activity of MNPs is significantly influenced by its morphology, Pd/NH_2-UiO-66(Zr), with Pd NPs deposited on the external surface of NH_2-UiO-66(Zr) was also prepared via a conventional single-solvent impregnation followed by a similar photoreduction process. As shown in Fig. S4, Pd nanoparticles with an average diameter of 8.6 nm, which is much larger than that observed over Pd@NH_2-UiO-66 (Zr), were deposited on the surface of NH_2-UiO-66(Zr). Although Pd/NH_2-UiO-66(Zr) also shows activity for the reaction between nitrobenzene and benzyl alcohol, only 59% of N-benzylaniline was obtained under the same conditions (Table 1, entry 7). It is proposed that the difference in the activities between Pd@NH_2-UiO-66(Zr) and Pd/NH_2-UiO-66(Zr) can be attributed both to the size and the position of the Pd NPs. As already well demonstrated, small size nanoparticles contain more unsaturated catalytic active sites [28,46–48]. Therefore, the small-sized Pd nanoparticles encapsulated inside the cavity should contain more coordinated unsaturated active Pd atoms than those supported on the surface of NH_2-UiO-66(Zr), which promote the hydrogenation of N-benzylideneaniline to produce N-benzylaniline. In addition, as already demonstrated in Pd/NH_2-UiO-66(Zr), the confinement of both Pd NPs and substrates in the cavities of NH_2-UiO-66(Zr) is beneficial for the rapid electron transfer from the excited NH_2-UiO-66(Zr) to Pd NPs to form electron-rich Pd species, which results in favorable activation of the substrates to realize an efficient light-induced synthesis of secondary amines [46].

In addition to the difference between the activity, Pd@NH_2-UiO-66 (Zr) and Pd/NH_2-UiO-66(Zr) show different stability during the reaction. Cycling test showed that there was no obvious loss of photocatalytic activity after three reaction runs over Pd@NH_2-UiO-66(Zr) (Fig. 4(a)) and both the XRD patterns and the TEM image of the used Pd@NH_2-UiO-66(Zr) did not show much change as compared with the fresh ones (Fig. 5(a) and 5(b)). ICP analysis revealed almost no detectable Pd in the filtrate. On the contrary, Pd/NH_2-UiO-66(Zr) show reduced activity during three runs (Fig. 4(b)). And although there is almost no change in the XRD pattern of the used Pd/NH_2-UiO-66(Zr) (Fig. S5(a)), its TEM shows aggregated Pd nanoparticles (Fig. S5(b)).

3.5. Investigations of the substrate scopes and the large scale reaction

The visible light initiated one-pot synthesis of secondary amines between nitrobenzene and benzyl alcohol over Pd@NH_2-UiO-66(Zr) was also expanded to a wide range of substrate scopes (Table 2). All investigated nitrobenzene derivatives can react with benzyl alcohol to produce the corresponding secondary amines after irradiated for 24 h, albeit with different yields. Nitrobenzene with electron-donating substituents such as p-OH and p-OCH_3 show slightly increased conversion ratios (96–98%) and comparable yields to secondary amines (83–87%) (Table 2, entries 2, 3), while electron-withdrawing group like -$COCH_3$ exhibit decreased conversion ratios (74%) and lower yield to secondary amines (66%) (Table 2, entry 4). Halogen-substituted nitrobenzene can also be converted to corresponding secondary amines with medium yield (50–61%) with no dehalogenation by-products detected (Table 2, entries 5, 6), which is particularly attractive since aryl halides usually dehalogenated over metal-based catalysts [49]. In addition, substituted benzyl alcohols can also react with nitrobenzene over Pd@NH_2-UiO-66 (Zr) under visible light, exhibiting medium to high yields (73–85%) to the corresponding secondary amines (Table 2, entries 7–9). Although the reaction can also be realized over aliphatic alcohols, lower yield of ca. 18% was obtained (Table 2, entry 10). Moreover, for all investigated reactions, the amount of aldehydes was always maintained at a high level, suggesting that using nitro compounds to replace amines in the N-alkylation reactions can effectively promote the dehydrogenation of alcohols, thereby promoting the whole tandem reaction to produce secondary amines.

The investigation of a large scale reaction is important considering the practical application. Therefore, a ten-fold scale-up reaction was also carried out. It was found that comparable nitrobenzene conversion (94%) as well as a high yield of 91% to N-benzylaniline was obtained (Table 1, entry 8). The result from the ten-fold reaction clearly demonstrated that an enlarged reaction is feasible.

4. Conclusion

In summary, we reported that Pd@NH_2-UiO-66(Zr), with small-sized Pd nanoparticles encapsulated inside the NH_2-UiO-66(Zr) cavities, can be an efficient and stable multifunctional catalyst to realize the one-pot syntheses of secondary amines by nitro compounds and alcohols under visible light. Using nitro compounds to replace the amines as the

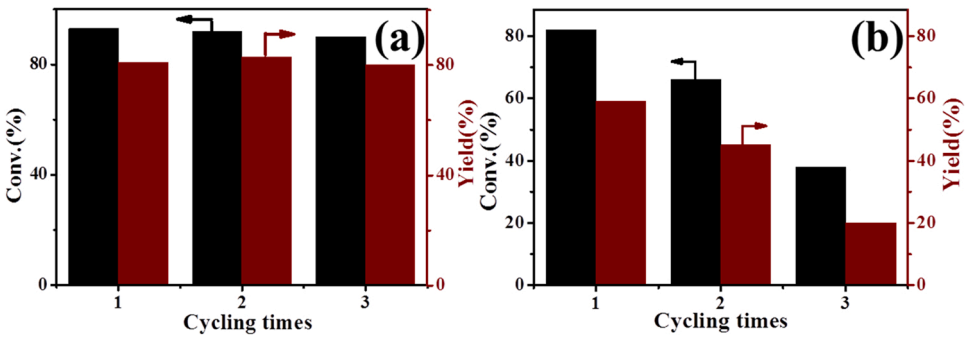

Fig. 4. (a) Cycling of Pd@NH_2-UiO-66(Zr) and (b) Pd/NH_2-UiO-66(Zr) for the synthesis of secondary amines by nitrobenzene and benzyl alcohol.

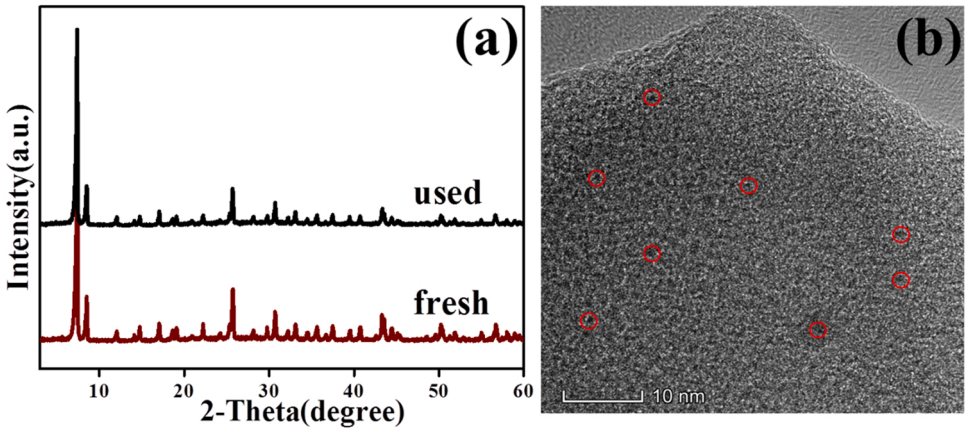

Fig. 5. (a) XRD patterns of Pd@NH_2-UiO-66(Zr) before and after reaction; (b) TEM image of the used Pd@NH_2-UiO-66(Zr).

Table 2
Photocatalytic syntheses of different secondary amines by nitro compounds and alcohols over Pd@NH_2-UiO-66(Zr).

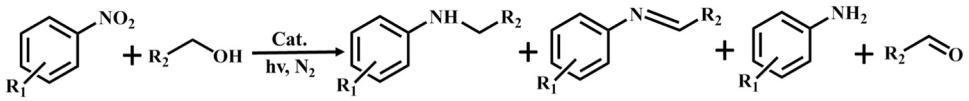

1a 2a 3a 3b 3c 3d

Entry.	Substrates		Conv. (%)	Yield. (%)			Aldehyde (μmol)
	R_1	R_2		3a	3b	3c	
1	H	Phenyl	93	81	5	4	2292
2	p-OH	Phenyl	96	83	7	5	2317
3	p-OCH_3	Phenyl	98	87	8	3	3251
4	p-$COCH_3$	Phenyl	74	66	2	5	1731
5	p-Cl	Phenyl	63	50	11	3	1253
6	p-Br	Phenyl	72	61	5	4	1562
7	H	p-Methoxyphenyl	94	82	9	1	2297
8	H	p-Methylbenzyl	96	85	8	2	3326
9	H	m-Methylbenzyl	92	73	15	4	2137
10	H	n-propyl	31	18	12	1	523

Reaction conditions: Pd@NH_2-UiO-66(Zr) 10 mg, nitro compound 0.1 mmol, alcohol 1 mL, CH_3CN 1 mL, N_2, irradiated for 24 h.

substrate can promote the dehydrogenation of alcohols since both photogenerated holes and electrons can be effectively consumed due to the coupling of dehydrogenation of the alcohols with hydrogenation of the nitro compounds. As compared with Pd/NH_2-UiO-66(Zr), Pd@NH_2-UiO-66(Zr) shows superior performance and higher stability during the reaction, illustrating the significant advantage of using the cavity of the MOFs as nanoreactor in controllable growth of small-sized metal nanoparticles. This study not only provides an efficient, green and cost effective strategy for the production of secondary amines, but also highlights the great potential of developing multifunctional MOFs based photocatalysts for one-pot tandem reactions.

Declaration of Competing Interest

The authors declare that they have no known competing financial interests or personal relationships that could have appeared to influence the work reported in this paper.

Acknowledgements

This work was supported by the NSFC (21872031 and U1705251). Z. L. thanks the Award Program for Minjiang Scholar Professorship for financial support.

Appendix A. Supporting information

Supplementary data associated with this article can be found in the online version at doi:10.1016/j.apcatb.2021.121031.

References

[1] D. Fiorito, S. Scaringi, C. Mazet, Transition metal-catalyzed alkene isomerization as an enabling technology in tandem, sequential and domino processes, Chem. Soc. Rev. 50 (2021) 1391–1406.
[2] C.T. Walsh, B.S. Moore, Enzymatic cascade reactions in biosynthesis, Angew. Chem. Int. Ed. 58 (2019) 6846–6879.
[3] S. Patra, N. Maity, Recent advances in (hetero)dimetallic systems towards tandem catalysis, Coord. Chem. Rev. 434 (2021), 213803.
[4] M. Hao, Z. Li, Visible light-initiated synergistic/cascade reactions over metal-organic frameworks, Sol. RRL 5 (2021), 2000454.
[5] S. Garbarino, D. Ravelli, S. Protti, A. Basso, Photoinduced multicomponent reactions, Angew. Chem. Int. Ed. 55 (2016) 15476–15484.
[6] Y.-B. Huang, J. Liang, X.-S. Wang, R. Cao, Multifunctional metal-organic framework catalysts: synergistic catalysis and tandem reactions, Chem. Soc. Rev. 46 (2017) 126–157.
[7] C.-X. Lü, G.-P. Zhan, K. Chen, Z.-K. Liu, C.-D. Wu, Anchoring Zn-phthalocyanines in the pore matrices of UiO-67 to improve highly the photocatalytic oxidation efficiency, Appl. Catal. B 279 (2020), 119350.
[8] X. Deng, Z. Li, H. García, Visible light induced organic transformations using metal-organic-frameworks (MOFs), Chem. Eur. J. 23 (2017) 11189–11209.
[9] Y. Shen, T. Pan, L. Wang, Z. Ren, W. Zhang, F. Huo, Programmable logic in metal-organic frameworks for catalysis, DOI: 10.1002/adma.202007442.
[10] J. Qiu, X. Zhang, Y. Feng, X. Zhang, H. Wang, J. Yao, Modified metal-organic frameworks as photocatalysts, Appl. Catal. B 231 (2018) 317–342.
[11] A. Dhakshinamoorthy, Z. Li, H. Garcia, Catalysis and photocatalysis by metal organic frameworks, Chem. Soc. Rev. 47 (2018) 8134–8172.
[12] Y. Yin, R. Lv, W. Zhang, J. Lu, Y. Ren, X. Li, L. Lv, M. Hu, B. Pan, Exploring mechanisms of different active species formation in heterogeneous Fenton systems by regulating iron chemical environment, Appl. Catal. B 295 (2021), 120282.
[13] J. Liu, L. Chen, H. Cui, J. Zhang, L. Zhang, C.-Y. Su, Applications of metal-organic frameworks in heterogeneous supramolecular catalysis, Chem. Soc. Rev. 43 (2014) 6011–6061.
[14] B. Li, M. Chrzanowski, Y. Zhang, S. Ma, Applications of metal-organic frameworks featuring multi-functional sites, Coord. Chem. Rev. 307 (2016) 106–129.
[15] G. Li, S. Zhao, Y. Zhang, Z. Tang, Metal-organic frameworks encapsulating active nanoparticles as emerging composites for catalysis: recent progress and perspectives, Adv. Mater. 30 (2018), 1800702.
[16] L. Jiao, Y. Wang, H.-L. Jiang, Q. Xu, Metal-organic frameworks as platforms for catalytic applications, Adv. Mater. 30 (2018), 1703663.
[17] Y. Qin, M. Hao, D. Wang, Z. Li, Post-synthetic modifications (PSM) on metal-organic frameworks (MOFs) for visible-light-initiated photocatalysis, DOI: 10.1039/D1DT02424H.
[18] M. Kalaj, S.M. Cohen, Postsynthetic modification: an enabling technology for the advancement of metal-organic frameworks, ACS Cent. Sci. 6 (2020) 1046–1057.
[19] Q. Yang, Q. Xu, H.-L. Jiang, Metal-organic frameworks meet metal nanoparticles: synergistic effect for enhanced catalysis, Chem. Soc. Rev. 46 (2017) 4774–4808.
[20] A. Dhakshinamoorthy, A.M. Asiri, H. Garcia, Metal organic frameworks as versatile hosts of Au nanoparticles in heterogeneous catalysis, ACS Catal. 7 (2017) 2896–2919.
[21] L. Chen, R. Luque, Y. Li, Controllable design of tunable nanostructures inside metal-organic frameworks, Chem. Soc. Rev. 46 (2017) 4614–4630.
[22] C.-D. Wu, M. Zhao, Incorporation of molecular catalysts in metal-organic frameworks for highly efficient heterogeneous catalysis, Adv. Mater. 29 (2017), 1605446.
[23] M. Wen, K. Mori, Y. Kuwahara, T. An, H. Yamashita, Design and architecture of metal organic frameworks for visible light enhanced hydrogen production, Appl. Catal. B 218 (2017) 555–569.
[24] T. Kitao, Y. Zhang, S. Kitagawa, B. Wang, T. Uemura, Hybridization of MOFs and polymers, Chem. Soc. Rev. 46 (2017) 3108–3133.
[25] Y. Liu, Z. Liu, D. Huang, M. Cheng, G. Zeng, C. Lai, C. Zhang, C. Zhou, W. Wang, D. Jiang, H. Wang, B. Shao, Metal or metal-containing nanoparticle@MOF nanocomposites as a promising type of photocatalyst, Coord. Chem. Rev. 388 (2019) 63–78.
[26] R.N. Salvatore, C.H. Yoon, K.W. Jung, Synthesis of secondary amines, Tetrahedron 57 (2001) 7785–7811.
[27] Y. Shiraishi, K. Fujiwara, Y. Sugano, S. Ichikawa, T. Hirai, N-Monoalkylation of amines with alcohols by tandem photocatalytic and catalytic reactions on TiO_2 loaded with Pd nanoparticles, ACS Catal. 3 (2013) 312–320.
[28] D. Wang, Z. Li, Coupling MOF-based photocatalysis with Pd catalysis over Pd@MIL-100(Fe) for efficient N-alkylation of amines with alcohols under visible light, J. Catal. 342 (2016) 151–157.
[29] L. Zhang, Y. Zhang, Y. Deng, F. Shi, Room temperature N-alkylation of amines with alcohols under UV irradiation catalyzed by Cu-Mo/TiO_2, Catal. Sci. Technol. 5 (2015) 3226–3234.
[30] D. Wang, Y. Pan, L. Xu, Z. Li, PdAu@MIL-100(Fe) cooperatively catalyze tandem reactions between amines and alcohols for efficient N-alkyl amines syntheses under visible light, J. Catal. 361 (2018) 248–254.
[31] L.-M. Wang, K. Jenkinson, A.E.H. Wheatley, K. Kuwata, S. Saito, H. Naka, Photocatalytic N-Methylation of amines over Pd/TiO_2 for the functionalization of heterocycles and pharmaceutical intermediates, ACS Sustain. Chem. Eng. 6 (2018) 15419–15424.
[32] B. Wang, Z. Deng, X. Fu, C. Xu, Z. Li, Photodeposition of Pd nanoparticles on $ZnIn_2S_4$ for efficient alkylation of amines and ketones' α-H with alcohols under visible light, Appl. Catal. B 237 (2018) 970–975.
[33] A.G. Siraki, in: J.C. Fishbein, J.M. Heilman (Eds.), Advances in Molecular Toxicology, Elsevier, 2013, pp. 39–82.
[34] B. Wang, Z. Deng, Z. Li, Efficient chemoselective hydrogenation of nitrobenzene to aniline, azoxybenzene and azobenzene over CQDs/$ZnIn_2S_4$ nanocomposites under visible light, J. Catal. 389 (2020) 241–246.
[35] X. Guo, C. Hao, G. Jin, H.-Y. Zhu, X.-Y. Guo, Copper nanoparticles on graphene support: an efficient photocatalyst for coupling of nitroaromatics in visible light, Angew. Chem. Int. Ed. 53 (2014) 1973–1977.
[36] C. Wu, C. Zhu, K. Liu, S. Yang, Y. Sun, K. Zhu, Y. Cao, S. Zhang, S. Zhuo, M. Zhang, Q. Zhang, H. Zhang, Nano-pyramid-type Co-ZnO/NC for hydrogen transfer cascade reaction between alcohols and nitrobenzene, DOI: 10.1016/j.apcatb.2021.120288.
[37] J. Song, Z.-F. Huang, L. Pan, K. Li, X. Zhang, L. Wang, J.-J. Zou, Review on selective hydrogenation of nitroarene by catalytic, photocatalytic and electrocatalytic reactions, Appl. Catal. B 227 (2018) 386–408.
[38] D. Sun, Z. Li, Robust Ti- and Zr-based metal-organic frameworks for photocatalysis, Chin. J. Chem. 35 (2017) 135–147.
[39] S. Yuan, J.-S. Qin, C.T. Lollar, H.-C. Zhou, Stable metal-organic frameworks with group 4 metals: current status and trends, ACS Cent. Sci. 4 (2018) 440–450.
[40] J.H. Cavka, S. Jakobsen, U. Olsbye, N. Guillou, C. Lamberti, S. Bordiga, K. P. Lillerud, A new zirconium inorganic building brick forming metal organic frameworks with exceptional stability, J. Am. Chem. Soc. 130 (2008) 13850–13851.
[41] A. Aijaz, A. Karkamkar, Y.J. Choi, N. Tsumori, E. Rönnebro, T. Autrey, H. Shioyama, Q. Xu, Immobilizing highly catalytically active Pt nanoparticles inside the pores of metal-organic framework: a double solvents approach, J. Am. Chem. Soc. 134 (2012) 13926–13929.
[42] B. Leipzig, Über stufenweise Reduktion des Nitrobenzols mit begrenztem Kathodenpotential, Z. Elektrochem. 4 (1898) 506–514.
[43] S. Roy, Photocatalytic Materials for Reduction of Nitroarenes and Nitrates, J. Phys. Chem. C 124 (2020) 28345–28358.
[44] K. Tsutsumi, F. Uchikawa, K. Sakai, K. Tabata, Photoinduced reduction of nitroarenes using a transition-metal-loaded silicon semiconductor under visible light irradiation, ACS Catal. 6 (2016) 4394–4398.
[45] S. Zhang, W. Huang, X. Fu, X. Zheng, S. Meng, X. Ye, S. Chen, Photocatalytic organic transformations: simultaneous oxidation of aromatic alcohols and reduction of nitroarenes on $CdLa_2S_4$ in one reaction system, Appl. Catal. B 233 (2018) 1–10.
[46] D. Sun, Z. Li, Double-solvent method to Pd nanoclusters encapsulated inside the cavity of NH_2-UiO-66(Zr) for efficient visible-light-promoted Suzuki coupling reaction, J. Phys. Chem. C 120 (2016) 19744–19750.
[47] D. Sun, M. Xu, Y. Jiang, J. Long, Z. Li, Small-sized bimetallic CuPd nanoclusters encapsulated inside cavity of NH_2-UiO-66(Zr) with superior performance for light-induced Suzuki coupling reaction, Small Methods 2 (2018), 1800164.
[48] T. Schalow, B. Brandt, D.E. Starr, M. Laurin, S.K. Shaikhutdinov, S. Schauermann, J. Libuda, H.-J. Freund, Size-dependent oxidation mechanism of supported Pd nanoparticles, Angew. Chem. Int. Ed. 45 (2006) 3693–3697.
[49] Y. Wang, Q. Zhu, Y. Wei, Y. Gong, C. Chen, W. Song, J. Zhao, Catalytic hydrodehalogenation over supported gold: electron transfer versus hydride transfer, Appl. Catal. B 231 (2018) 262–268.